# Spin Density Distribution and Energy Stabilization in the Cation Radicals of Multilayered Compounds

Hiroaki OHYA-NISHIGUCHI,* Atsushi TERAHARA, Noboru HIROTA, Yoshiteru SAKATA,† and Soichi MISUMI†

*Department of Chemistry, Faculty of Science, Kyoto University, Kyoto 606*

†*The Institute of Scientific and Industrial Research, Osaka University, Osaka 565*

(Received November 6, 1981)

The spin density distributions and the energy stabilizations in the polymer cation radicals ($R_n^{+\cdot}$) have been investigated by measuring the oxidation potentials ($E^\circ_{1/2}$) and the electron spin resonance (ESR) spectra of the cation radicals generated by the electrochemical oxidations of some multilayered compounds. $E^\circ_{1/2}$ decreased monotonically as the number of layers increased. The spin densities on the aromatic rings have been estimated from the hyperfine coupling constants with the help of the McLachlan's and INDO calculation. It was found that the spin density tends to localize in the central moieties in $R_n^{+\cdot}$. The localization of the spin density and the energy stabilization are interpreted with a simple theoretical model of $R_n^{+\cdot}$, which takes into accounts the repulsion integral ($\gamma_1$) and resonance integral ($\zeta$) between the nearest neighbor molecules. The comparison with the experimental data has lead to the numerical estimates of $\gamma_1=0.1$ eV and $\zeta=0.4$ eV.

The dimer cation radicals ($R_2^{+\cdot}$) of some aromatic hydrocarbons are known to be formed by the reaction

$$R^{+\cdot} + R \rightleftharpoons R_2^{+\cdot}, \quad (1)$$

when R are partly oxidized chemically in liquid solution,[1] by high energy irradiation in solid solution,[2] or by chemical reaction in gaseous state.[3] Such dimer cations have been characterized by negative enthalpies of formation, spin densities equally distributed over the two moieties, and eclipsed configurations in the dimers. The negative enthalpies are possibly due to the transannular interaction between the moieties which stabilizes the dimer species.

Higher polymeric radical species $R_n^{+\cdot}$ may be formed successively by the reaction scheme

$$R_{n-1}^{+\cdot} + R \rightleftharpoons R_n^{+\cdot}, \quad (2)$$

if the enthalpy difference between $R_n^{+\cdot}$ and $R_{n-1}^{+\cdot}$ is much larger than $kT$ and sufficient concentration of R is present. In agreement with this expectation we previously succeeded in obtaining the ESR spectrum of coronene trimer cation radical $C_3^{+\cdot}$.[1m] It was shown from the spectrum analysis that the ratio between the spin densities in the central molecule and those in the side molecules is 6 : 1 in contrast to the 2 : 1 ratio predicted by the HMO calculation. This difference was attributed to the effect of transannular interaction.

The cation radicals of multilayered compounds such as paracyclophanes can be regarded as suitable model compounds for $R_n^{+\cdot}$ in clarifying characteristic features of $R_n^{+\cdot}$ arising on polymer formation. Anthracenophane cation radical, for example, was found to be a good model of anthracene dimer cation radical.[1k]

For an ESR study of the cation radicals of multilayered compounds, electrochemical generation has some advantages over the usual chemical methods or high energy irradiation: One is that the radical generation can easily be controlled by application of a proper voltage comparable to $E^\circ_{1/2}$ of the compound under consideration from outside the ESR system. One of the present authors (H.O.) recently developed a simple two-electrode cell using a helix which is very advantageous over the commonly used electrolysis cell in obtaining the spectra of unstable radical cations.[4] In this work, we have used this cell in studying ESR spectra of the radical cations of some multilayered compounds.

Although the ESR study of the multilayered compounds provide valuable information about their electronic wave functions constructed from those of constituting moieties, the information about their orbital energies is not obtained directly. On the other hand, cyclic voltammetry (CV) is an efficient and convenient method in obtaining the oxidation and reduction potentials associated with removal of an electron from the highest occupied molecular orbital (HOMO) and addition to the lowest unoccupied molecular orbital (LUMO), respectively. We have attempted to estimate the magnitude of transannular interactions from measurements of redox potentials.

In this paper we first report the results of electrochemical measurements of the several compounds **1** to **5** in Fig. 1 in relation to the dependence of the oxidation

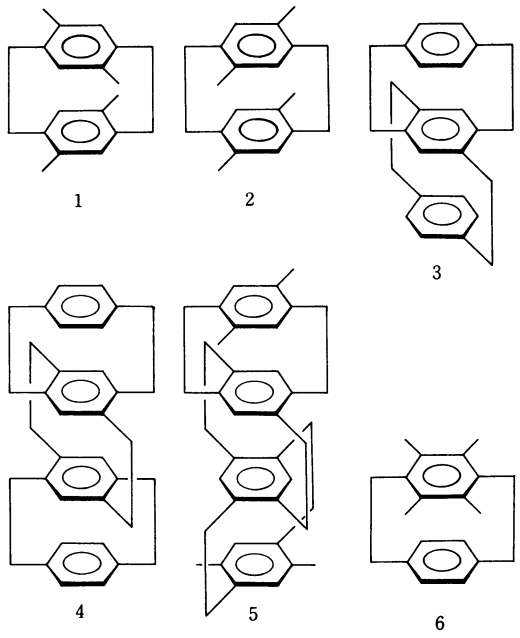


Fig. 1. Molecular structures of the multilayered compounds investigated.

potentials on the number of aromatic layers. Secondly, the ESR results of the cation radicals of these compounds are shown, and compared with those of $R_2^{+\cdot}$ and $R_3^{+\cdot}$ so far investigated. The MO calculations of the multilayered compounds were carried out using McLachlan's and INDO methods in order to interpret the observed spectra. Thirdly, we present a theoretical treatment of the spin distribution and energy stabilization in the multilayered aromatic systems, which takes into account repulsion and resonance integrals between the nearest neighbor molecules.

The model compounds such as those treated here are more amenable to detailed ESR investigations than the clustering intermediates produced in the course of chemical and biochemical reactions. Therefore, definitive ESR characterization of the multilayered compounds provides a framework for further understanding of the clustering intermediates in the chemical reactions.

## Experimental

Substances shown in Fig. 1 were synthesized according to the methods described previously.[5,6] Commercially available hexamethylbenzene (**H**) and durene (**D**) were used without further purification. Purified and dried dichloromethane ($CH_2Cl_2$) or butyronitrile (BuCN) and tetrabutylammonium tetrafluorobotate (TBFB) of special grade for polarography were used as solvents and a supporting electrolyte, respectively. The cyclic voltammograms of the compounds, **1** to **5**, **H**, and **D**, were measured using a PAR 173 potentio/galvanostat equipped with an I/V converter, PAR 176, in conjunction with a Hewlett-Packard 3310A function generator. As a pseudo reference electrode a silver wire was used. In order to avoid the ambiguity of the potential of the reference electrode, a small amount of ferrocene was added and the position of the waves of the compounds under consideration were directly compared to that of ferrocenium/ferrocene ($Fc^+/Fc$) couple (0.400 V *vs.* NHE) used as an internal standard.[7] The electrochemical oxidation of the compounds for ESR measurements was carried out in the cavity using a helical working electrode made of gold wire. The details of the cell construction and the experimental procedure were given previously.[4] The appearance voltage, $V_a$, at which the ESR signal with modiulation amplitude of 1 G†† appears, was measured before the observation of high resolution spectra. The ESR spectra were measured with a JEOL FE-3X spectrometer, equipped with a temperature controller. Potassium nitrosylbis(sulfate) was used as a standard sample for the calibration of the magnitude and interval of the magnetic field, the accuracy of the latter being 0.005 G.

## Results

*The Appearance Voltages and the Oxidation Potentials of the Multilayered Compounds.* $V_a$ were measured at low temperatures at which the ESR spectra were also obtained (−70 °C to −90 °C). On the other hand, the $E^\circ_{1/2}$ were estimated from the peak potentials appeared on the anodic and cathodic sweeps (100 mV/s) by the usual method. $V_a$ and $E^\circ_{1/2}$ of **3** to **5** nicely coinsided with each other in the range of experimental errors, but $V_a$ of **1** and **2** become appreciably high compared with the corresponding $E^\circ_{1/2}$. This is probably due to the instability of the cation radicals produced, as pointed out in the previous paper.[4] It can be seen from Table 1 that both $V_a$ and $E^\circ_{1/2}$ decrease as the number of the aromatic rings in the molecule $n$ increases. In addition, $E^\circ_{1/2}$ of **1** showed an appreciable decrease from $E^\circ_{1/2}$ of **D**. This suggests the importance of the transannular interaction between the two moieties in spite of their configulation with a small overlap integral.

*ESR Spectra of $1^{+\cdot}$ and $2^{+\cdot}$.* After the temperature of the solution of **1** was decreased as low as −85 °C, the voltage applied between the two electrodes was increased step by step, while observing the ESR signal on an oscilloscope or a recorder. At 1.6±0.1 V well separated 13 lines with the relative intensity ratios of combinations of $_{12}C_r$ appeared. When the modulation amplitude was decreased as low as 0.063 G, each line was further split into well resolved 25 lines as shown in Fig. 2a. The analysis of this spectrum and assignment of the hfcc obtained were straight forward because of different

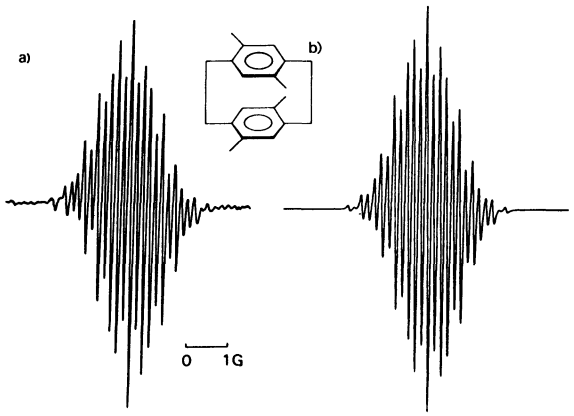


Fig. 2. One of well separated 13 groups due to the methylgroups in the ESR spectra of $1^{+\cdot}$; (a): observed (b): simulated.

Table 1. The appearance voltages ($V_a$) and the oxidation potentials of **1** to **5** in addition to those of durene (**D**), hexamethyl benzene (**H**), and paracyclophane (**P**)

| | **D** | **H** | **P** | **1** | **2** | **3** | **4** | **5** |
|---|---|---|---|---|---|---|---|---|
| $V_a$/V[a] | — | — | — | 1.6 | 1.4 | 1.1 | 0.8 | 0.8 |
| $E^\circ_{12}$/V[b] | 1.67[c] | 1.52[c] | 1.40[c] | 1.24[d] | 1.13[e] | 1.07[e] | 0.83[e] | 0.80[e] |

a) Voltages at which the ESR signals appear at −70 °C to − 90 °C. Solvent: $CH_2Cl_2$+$CF_3COOH$ (10 : 1), with $TBAPF_6$. b) ($E^\circ_{1/2}$ *vs.* NHE)/V were estimated from $(V^O+V^R)/2$ *vs.* the peak potential of ferrocene (0.400 V *vs.* NHE). Solvents: BuCN or $CH_2Cl_2$, with $TBAPF_6$. c) Irreversible. d) Quasireversible. e) Reversible.

†† 1 G = $10^{-4}$ T.

numbers of the equivalent protons: 6.486 G for twelve methyl-protons, 0.486 G for eight bridge-protons, and 0.334 G for four ring-protons.

The ESR signals of $\mathbf{2}^{+\cdot}$ similar to that of $\mathbf{1}^{+\cdot}$ appeared at $-70$ °C at $1.4\pm0.1$ V which was 0.2 V lower than that of **1**. The resolution of each group of lines is poorer than in the case of $\mathbf{1}^{+\cdot}$ because of the small difference between the two small hfcc: 6.365 G for twelve methyl-protons, 0.41 G for eight bridge-protons, and 0.43 G for four ring-protons.

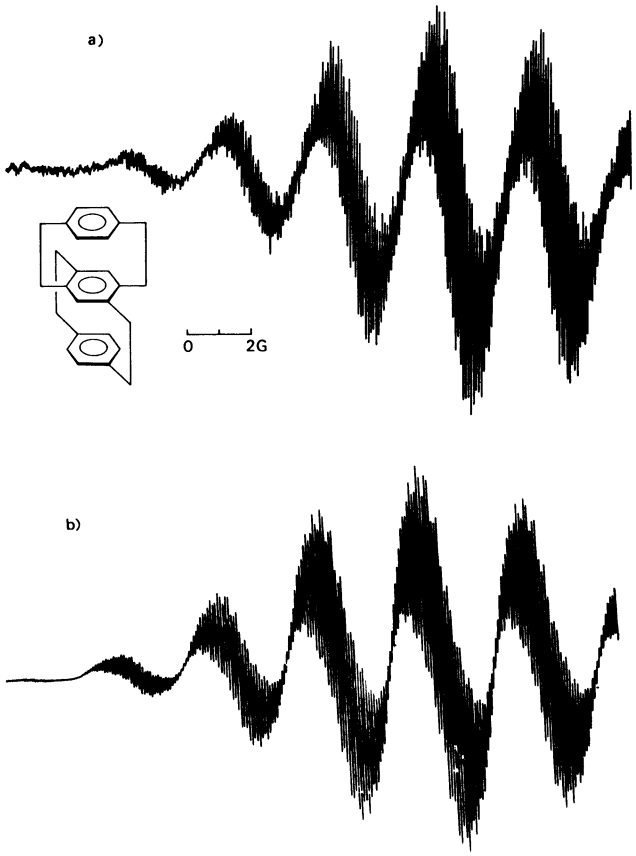


Fig. 3. The observed (a) and simulated (b) ESR spectra of $\mathbf{3}^{+\cdot}$.

*The ESR Spectrum of* $\mathbf{3}^{+\cdot}$. The well resolved spectrum of $\mathbf{3}^{+\cdot}$ was obtained at $-56$ °C (Fig. 3a). $V_a$ (1.1 V) was lower than those of **1** and **2**. The obtained spectrum was very complex, but resolved well enough to be analyzed completely by computer simulation (Fig. 3b). 0.789 G due to two equivalent protons can be assigned unequivocally to the ring protons in the central ring in **3**. The larger hfcc, 3.279 and 3.049 G, due to two groups of equivalent four protons were not assigned uniquely, but assigned tentatively to the two four-equivalent bridge protons close to the central ring. The other hfcc can be attributable to the protons attached to the two side rings.

*The ESR Spectra of* $\mathbf{4}^{+\cdot}$ *and* $\mathbf{5}^{+\cdot}$. At $-85$ °C the ESR signals of both compounds appeared at $0.8\pm0.1$ V, which is 0.3 V lower than that of $\mathbf{3}^{+\cdot}$. They showed only one broad Gaussian-type line with the linewidths of 5.6 and 4.5 G, respectively. These radical species were very stable compared with the other species described above.

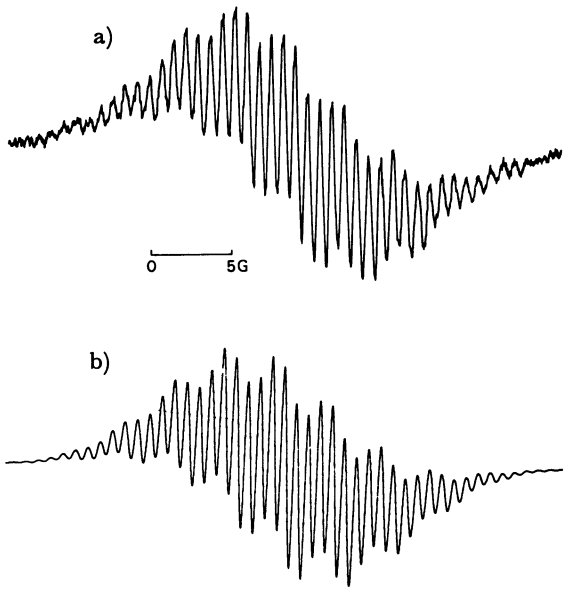


Fig. 4. The observed (a) and simulated (b) ESR spectra due to $\mathbf{1}_2^{+\cdot}$ at $-112$ °C.

*The ESR Spectrum of* $\mathbf{1}_2^{+\cdot}$. When a solution of **1** was oxidized at higher concentration and the lowest temperature available, $-112$°C, we observed a spectrum different from that of $\mathbf{1}^{+\cdot}$ (Fig. 4a). The conditions for obtaining this spectrum, a) high concentration, b) low temperature, and c) the beginning of the electrolysis, coincided with those for production of the dimers of typical aromatic hydrocarbons.[4] Figure 4b was obtained by the coupling constants: 3.074 G and 0.768 G for twelve-equivalent protons, and the additional unresolved couplings, 0.177 and 0.138 G for eight- and four-equivalent protons, respectively, using the Lorential lines of the widths of 0.380 G. The agreement between the simulated spectrum and the observed one is good enough to conclude that the spectrum is due to the dimer cation radical $\mathbf{1}_2^{+\cdot}$, formed according to Eq. 1. The hfcc of 3.074 G and 0.768 G are due to two different types of methyl protons, which indicates that spin densities on the central and the side rings are very different; the ratio being 4.0 : 1.

*Comparison of the Hfcc with MO Calculations.* Detailed molecular orbital calculations of paracyclophane and related compounds have been reported by many investigators.[8] In order to interpret the observed spectra, we have calculated hfcc by the McLachlan's and INDO methods. The usefulness of the McLachlan's method in calculating the hfcc of ordinary aromatic radical ions is well established. We have applied this method to the multilayered compounds taking into account of inter-ring interactions.

In Fig. 5 are shown the simplified molecular models (**1′** to **3′**) for **1** to **3**, used for calculation. Effects of the ethylene bridges are taken into consideration by changing the Coulomb integrals of the carbons in the rings as $\alpha(C')=\alpha_C-0.1\beta$. In our case the observed hfcc due to the methyl protons suggest a large effect of hyperconjuga-

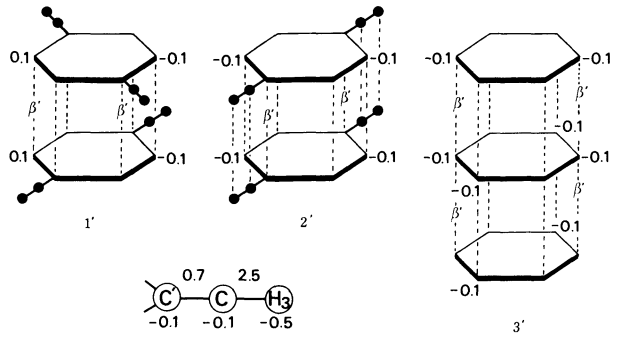


Fig. 5. The simplified molecular models, **1'**, to **3'**, for **1** to **3**, used for McLachlan's MO calculation.

tion. Therefore, the values of the Coulomb and resonance integrals of the methyl group C'–C≡$H_3$ were chosen as $\alpha(C')=\alpha(C)=\alpha_C-0.1\beta$, $\alpha(H_3)=\alpha_C-0.5\beta$, $\beta(C'-C)=0.7\beta$, and $\beta(C-H_3)=2.5\beta$ (hyperconjugation model[9]). In addition to those values the resonance integrals between the atoms of the upper and lower moieties in the molecule ($\beta'$) were included only for pairs of carbon atoms $C^l$ and $C^u$ that lie on top of one another, as shown in Fig. 5. The interactions between the methyl groups in **2'** were also included.

$Q$ values for estimating the hfcc from the calculated spin densities are somewhat ambiguous because 1) the layered configurations of the $\pi$-orbitals yield direct overlap of H atoms in the one moiety with the $\pi$-electron cloud of the other moiety, 2) each moiety does not have a planer structure, and 3) the exact configurations of the bridge protons are not known. In Table 2 are listed the hfcc calculated by this method using the following equations;

$$a_H = -24\rho_{C'} \quad \text{for ring protons,}$$

$$a_H^{CH_3} = 170\rho_{H_3} + 25\rho_{C'} \quad \text{for methyl protons, and}$$

$$a_H^{CH_2} = 6.3\rho_{C'} \quad \text{for bridge protons.}$$

The $Q$ values for the bridge protons were estimated by $Q=50\cos\theta$,[10] where $\theta$ was calculated based on the crystallographic data of paracyclophane.[11]

Figure 6 shows the hfcc of $\mathbf{1}^{+\cdot}$ and $\mathbf{2}^{+\cdot}$ calculated as functions of $\beta'$. The dependences of the hfcc on $\beta'$ are remarkably different in the two molecules. It can be seen that the hfcc of the ring protons in $\mathbf{1}^{+\cdot}$ drastically changes from 0.65 to −3.10 G as $\beta'$ increases. At $\beta'=0.03\,\beta$ the theoretical hfcc due to three kinds of protons are all in reasonably good agreements with the experimental values given in Table 2. On the other hand, the hfcc of $\mathbf{2}^{+\cdot}$ are independent of the variation of $\beta'$. Calculated values are in good agreement with the observed ones.

The hfcc of $\mathbf{3}^{+\cdot}$ were calculated in the similar manner as in the case of $\mathbf{1}^{+\cdot}$ and $\mathbf{2}^{+\cdot}$. The best fit was obtained at $\beta'=0.04\,\beta$. The calculated values are also shown in Table 2. The largest and the second largest hfcc in the experimental data were well reproduced by those due to the bridge protons close to the central ring in spite of many ambiguities described above. The spin density is extremely localized on the central ring to those on the side rings being about 15 : 1.

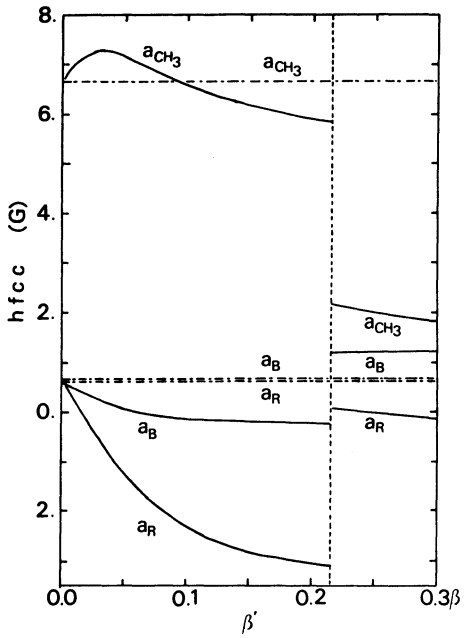


Fig. 6. The $\beta'$ dependences of the hfcc of $\mathbf{1}^{+\cdot}$ and $\mathbf{2}^{+\cdot}$. ——: $\mathbf{1}^{+\cdot}$, -·-·-: $\mathbf{2}^{+\cdot}$.

Table 2. The observed and calculated hyperfine coupling constants of $\mathbf{1}^{+\cdot}$, $\mathbf{2}^{+\cdot}$, $\mathbf{3}^{+\cdot}$, and $\mathbf{1}_2^{+\cdot}$

| | Obsd (G) | Calcd (G) | | |
|---|---|---|---|---|
| | | McLachlan | | INDO |
| $\mathbf{1}^{+\cdot}$ | (12H) 6.486 | 7.254 | | 8.772 |
| | (8H) 0.486 | −0.569 | | −0.353 |
| | (4H) 0.334 | 0.279 | | 0.769 |
| $\mathbf{2}^{+\cdot}$ | (12H) 6.365 | 6.668 | | |
| | (8H) 0.41 | 0.662 | | |
| | (4H) 0.43 | 0.646 | | |
| | | | (Case 1)[a] | (Case 2)[a] |
| $\mathbf{3}^{+\cdot}$ | (4H) 3.279 | 3.201 | 6.330 | 4.910 |
| | (4H) 3.039 | | 4.672 | 3.462 |
| | (2H) 0.789 | 1.487 | 2.563 | 1.660 |
| | (4H) 0.320 | −0.858 | −0.468 | −0.706 |
| | (4H) 0.238 | | −0.620 | −0.859 |
| | (9H) 0.091 | 1.410 | −0.023 | 0.031 |
| | | 0.772 | −0.018 | 0.141 |
| $\mathbf{1}_2^{+\cdot}$ | (12H) 3.074 | | | |
| | (12H) 0.768 | | | |
| | (8H) 0.177 | | | |
| | (4H) 0.138 | | | |

a) See text.

The hfcc of $\mathbf{1}^{+\cdot}$ and $\mathbf{2}^{+\cdot}$ were also calculated by the INDO method. The positions of the atoms in **1** were derived from the crystallographic data of paracyclophane.[11] In addition, we adopted a trial configuration in which the C–C bond connecting the methyl groups to the aromatic rings are parallel to the C–H bond of paracyclophane and one of the C–H bonds in the methyl group is equatorial about the rings. The hfcc of the methyl protons are averaged after the calculation because the rotations of the methyl groups about the C–C bonds are usually fast. The INDO calculation also gives the same trend of the spin distribution as

obtained by the McLachlan's method, but the numerical agreements are somewhat poorer. The main cause of the discrepancy may be due to the difference between the actual structure of $\mathbf{1}^{+\cdot}$ and that of paracyclophane.

In the INDO calculation of $\mathbf{3}^{+\cdot}$ the positions of the atoms in **3** were first derived from the crystallographic data of brominated **3** (Case 1).[12] In the second trial we used a structure in which the distance between the central moiety and the side ones were shortened by 0.2 Å (Case 2). The 1.25 A C–H bond length of the central ring protons derived crystallographically was also changed to the usual C–H bond distance of 0.98 Å in Case 2. The agreements between the experimental and calculated hfcc are poor in Case 1, but considerable improvement was achieved in Case 2. Although the largest hfcc obtained in Case 2 is large, the INDO result is in agreement with the result obtained by the McLachlan's calculation with $\beta'=0.04\,\beta$. The INDO result in Case 1 resembles to the McLachlan's result with $\beta'$ smaller than $0.01\,\beta$. This may suggest that on the formation of the cation radical two side moieties are contracted to the central moiety, leading to the increased spin densities on the side moieties. The number of the atoms in **4** and **5** were too large to carry out the INDO calculations.

## Theoretical Model of $R_n^{+\cdot}$

When two or more aromatic rings are stucked face to face, some transannular interactions are expected between $\pi$-electronic systems. As the whole they constitute an aggregate $R_n$. The spin density of $R_n^{+\cdot}$ is related to the highest occupied molecular orbital (HOMO) of $R_n$ which are constructed by the HOMO of constituting molecules. In the following, therefore, we only consider the HOMO $\phi_i(i=1$ to $n)$ of $i$-th molecule in $R_n$, which is doubly occupied by $\pi$-electrons. The total energy of $R_n$ can be generally given by

$$E_0^n = \int \Psi_0 \boldsymbol{H} \Psi_0 d\tau = 2\sum_i^n H_{ii} + \sum_i^n \sum_j^n (2J_{ij} - K_{ij}), \quad (3)$$

where $H_{ij}$, $J_{ij}$, and $K_{ij}$ have the usual meanings.[13] Assuming that an electron is removed from $\phi_i$, a configuration $\Psi_i$ of $R_n^{+\cdot}$ is written as $\Psi_i=|\phi_1^2\phi_1^2\cdots\phi_i^1\cdots\phi_n^2|$ and the ground state wave function $\Psi_G^n$ of $R_n^{+\cdot}$ is expressed by a linear combination of $n$ configurations:

$$\Psi_G{}^n = \sum_{i=1}^n C_i \Psi_i, \quad (4)$$

where $C_i$ is the coefficient of the linear combination, and $C_i^2$ corresponds to the spin density on the $i$-th molecule. In order to derive the ground state energy $E_G{}^n$, one need to solve

$$(\boldsymbol{H} - E\boldsymbol{1})\boldsymbol{C} = 0, \quad (5)$$

where $\boldsymbol{H}$ is the hamiltonian matrix defined by

$$H_{ij} = \langle \Psi_i | \boldsymbol{H} | \Psi_j \rangle. \quad (6)$$

$\boldsymbol{1}$ is the unit matrix, and $\boldsymbol{C}$ is the column vector which consists of $C_i$ $(i=1$ to $n)$. The diagonal elements of the matrix $H_{ii}$ can be simply expressed in reference to $E_0{}^n$ as

$$H_{ii} = E_0{}^n - H_{ii} - \sum_j^n \{2J_{ij} - K_{ij}\}. \quad (7)$$

We assume that $J_{ij}$ and $K_{ij}$ have non zero values only when $j=i$ $(i=1$ to $n)$ and $j=i\pm1$ $(i=2$ to $n-1)$ and replace $J_{ii}$ and $J_{i\,i+1}$ by $\gamma_0$ and $\gamma_1$. Then

$$H_{ii} = E_0{}^n - H_{ii} - \gamma_0 - 2\gamma_1 \quad \text{for } i = 1 \text{ and } n, \quad (8)$$

$$H_{ii} = E_0{}^n - H_{ii} - \gamma_0 - 4\gamma_1 \quad \text{for } i = 2 \text{ to } n-1. \quad (9)$$

The off diagonal elements $H_{ij}$ is also assumed as

$$H_{ij} = \zeta \quad \text{for } j = i \pm 1, \quad (10)$$

$$H_{ij} = 0 \quad \text{for others.} \quad (11)$$

By substituting $H_{ij}$ into Eq. 5, one can derive the determinant $D_n$ as

$$D_n = \begin{vmatrix} -2\gamma_1-\varepsilon & \zeta & 0 & \cdots & 0 \\ \zeta & -4\gamma_1-\varepsilon & \zeta & \cdots & 0 \\ 0 & \zeta & -4\gamma_1-\varepsilon & \cdots & 0 \\ \cdots & \cdots & \cdots & \cdots & \cdots \\ 0 & 0 & 0 & & -2\gamma_1-\varepsilon \end{vmatrix} = 0, \quad (12)$$

where

$$\varepsilon = -E_0{}^n + H_{ii} + \gamma_0 - E. \quad (13)$$

It is convenient to rewrite $D_n$ by using $\theta$ and $\alpha$ defined by

$$-4\gamma_1 - \varepsilon = \zeta \cdot 2\cos\theta, \quad (14)$$

$$\gamma_1 = \alpha\zeta. \quad (15)$$

Then

$$D_n = \zeta^n \begin{vmatrix} 2\cos\theta + 2\alpha & 1 & 0 & \cdots & 0 \\ 1 & 2\cos\theta & 1 & \cdots & 0 \\ 0 & 1 & 2\cos\theta & \cdots & 0 \\ \cdots & \cdots & \cdots & \cdots & \cdots \\ 0 & 0 & 0 & \cdots & 2\cos\theta+2\alpha \end{vmatrix} = 0. \quad (16)$$

$D_n$ can be expanded into a polynomial of $\cos\theta$ expressed as

$$D_n = \frac{\zeta^n(-1)^{n-2}}{\sin\theta} \times \{\sin(n+1)\theta - 4\alpha\sin n\theta + 4\alpha^2\sin(n-1)\theta\} = 0. \quad (17)$$

From this equation one can obtain $n$ solutions $\theta_k(k=1$ to $n)$ which lead to

$$E_G{}^n = E_0 - H_{ii} - \gamma_0 - 4\gamma_1 + 2\zeta\cos\theta_1, \quad (18)$$

$$\Psi_G{}^n = A\sum_i \{\sin i\theta_1 - 2\alpha\sin(i-1)\theta_1\}\phi_i. \quad (19)$$

It should be noted that the transannular interaction $(E_G^n - E_G^1)$ is given as a sum of the repulsion and the resonance integrals.[14] The spin density distribution at the $i$-th molecule is finally derived as

$$\rho_i = A^2\{\sin i\theta_1 - 2\alpha\sin(i-1)\theta_1\}^2. \quad (20)$$

In Fig. 7 the ratio of the spin densities of the central moieties to those of the side ones plotted as functions of $\alpha$ for the cases of $n=3$ and $n=4$.

As $n\to\infty$, the stabilization energy in reference to $R_1{}^{+\cdot}$, $H_n=E_G{}^n-E_G{}^1$, converges to $-4\gamma_1+2\zeta$. In Fig. 8 $2\cos\theta_1$ is plotted as a function of $n$. As $n$ approaches infinity this quantity converges to 2, as can be seen from Eq. 18. On the other hand, in the limit of $\zeta=0$, Eqs. 18 and 19 are reduced to the following equations which

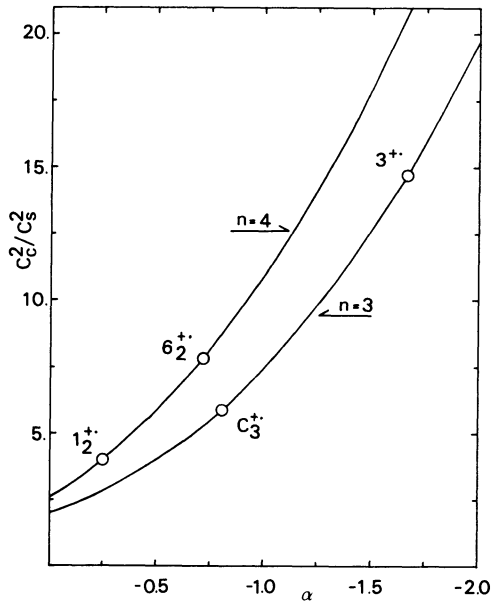


Fig. 7. The ratio of the spin densities of the central moieties to those of the side ones plotted as functions of $\alpha$ for the cases of $n=3$ and $n=4$.

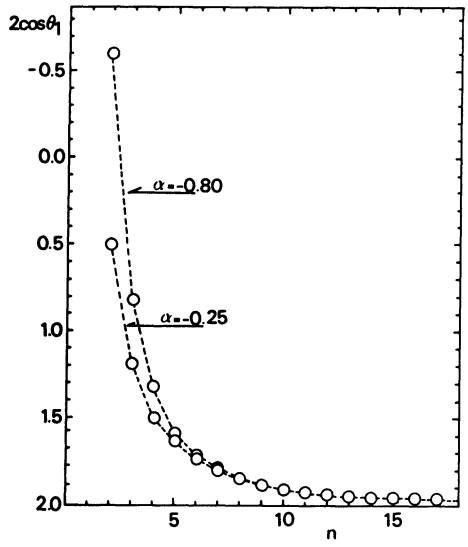


Fig. 8. $2\cos\theta_1$ plotted as functions of $n$ for $\alpha=-0.25$ and $-0.80$.

are derived for the chain molecules in the Hückel treatment:[15]

$$E_j = \gamma_0 + 2\zeta\cos\theta_j, \tag{22}$$

$$\Psi_j = A\sum_i \sin i\theta_j\cdot\phi_i, \tag{23}$$

with

$$\theta_j = \frac{\pi\cdot j}{n+1}\,. \tag{23}$$

It should be noted in Eq. 16 that even in the case of $R_n^{+\cdot}$ in which two end molecules are different from others the determinant similar to Eq. 16 can be derived. Therefore, one can use Eqs. 18 and 19 even in the case of **3**, adjusting the parameter which includes the energy difference $H_{ii}-H_{jj}$.

## Discussion

*The Energy Stabilization.* $V_a$ and $E^\circ_{1/2}$ of **1** to **5** decrease in the order of **1** to **5**. This trend is consistent with that of Fig. 8 derived theoretically from Eq. 18. It is of interest to examine the magnitude of the transannular interaction of each compound in relation to this trend.

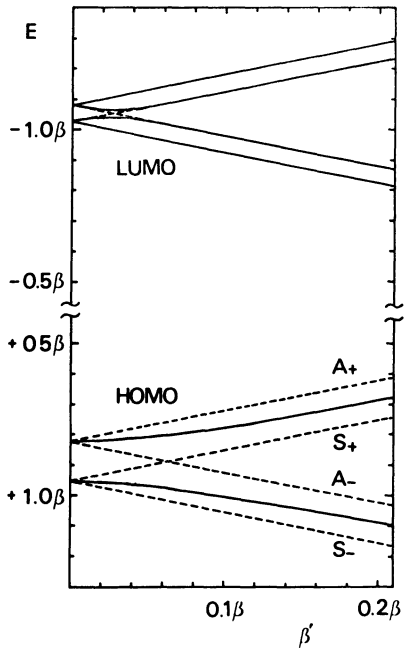


Fig. 9. $\beta'$ dependences of some orbital energies including the HOMO and the LUMO calculated by HMO method; for **1** (——) and **2** (------).

Figure 9 shows $\beta'$ dependence of some orbital energies including the HOMO and the LUMO of **1** and **2** calculated by the HMO method. The degenerate benzene orbitals, A and S ($e_{1u}$), have nodal planes perpendicular to each other, which are also perpendicular to the benzene plane. These orbital energies are split into two by substituting methyl and methylene groups to two benzene rings which results in **1** or **2**. The orbital energy of A is higher than that of S. As the transannular interaction between the two moieties $M_u$ and $M_l$ increases, each orbital of **2** splits further into two orbitals which are given as

$$A^{\pm} = (A^u \pm A^l)/2,$$

$$S^{\pm} = (S^u \pm S^l)/2. \tag{24}$$

The HMO and McLachlan's calculations of $\mathbf{2}^{+\cdot}$ show constant hfcc (Fig. 6) and linear change of the HMO energy with respect to the increase of $\beta'$. $\mathbf{2}^{+\cdot}$ corresponds to the usual dimeric species $R_2^{+\cdot}$ of the typical aromatic hydrocarbons with eclipsed configuration.

On the other hand, the energies of $A^+$ and $A^-$ ($S^+$ and $S^-$) of **1** are almost degenerate in all range below 0.2 $\beta$, because the twisting configuration of the two moieties reduces the resonance energy between the moieties,

but an orbital mixing between $A^{\pm}$ and $S^{\pm}$ occurs through the transannular interaction. Such a mixing in **1** causes the spin density redistribution in each moiety and the lifting of the HOMO energy, as shown in Fig. 9.

The oxidation potential of durene was measured as 1.67 V. **1** consists of two durene moieties rotated each other by about 60°. Since the resonance stabilization of **1** is almost zero, one can roughly estimate the value of $\gamma_1$ using Eq. 18. As the measured value of $E^{\circ}_{1/2}$ of **1** is 1.24 V, the difference with that of durene, 0.43 V, is equal to $4\gamma_1$. Then $\gamma_1$ is estimated to be 0.11 eV. Since the interlayer distance of the compounds measured here do not change much, $\gamma_1$ of these compounds may be regarded to be the order of this magnitude.

$E^{\circ}_{1/2}$ of **2** is 0.11 V lower than that of **1**. This means that the eclipsed configuration of drurene in **2** results in an appreciable resonance interaction between the two moieties. Using Eq. 18, the difference between $E^{\circ}_{1/2}$ of **1** and that of **2** is given to be $2\zeta \cos\theta_1$, from which we can derive the numerical value of $\zeta$ provided that $2\cos\theta_1$ is estimated experimentally.

The dimeric species of **1**, $\mathbf{1}_2^{+\cdot}$, exhibited clear hf splittings with the ratio of two kinds of hfcc due to the methyl groups being 4 : 1. Assuming that the four aromatic rings in $\mathbf{1}_2^{+\cdot}$ are stacked face to face and the interactions among four moieties are equal, we obtain $a=-0.25$ from this ratio with $n=4$ in Eq. 20. As $\gamma_1$ is of the order of 0.1 eV, $\zeta$ is estimated to be 0.4 eV from Eq. 15. Alternatively, the difference between $E^{\circ}_{1/2}$ of **1** and that of **2**, 0.11 V corresponds to $2\zeta\cos\theta_1$. Substituting $a=-0.25$ into Eq. 18, we obtain $2\cos\theta_1=0.50$ and $\zeta=0.22$ eV. $\zeta$ estimated by these two different methods are in the same order of magnitude.

The $\pi$ system of **3** consists of one durene at the center and two *p*-xylenes at both sides. The HOMO of *p*-xylene and durene are A and S respectively, each of which has a nodal plane rotated by 30° from each other. Therefore the resonance interaction is to be rather small, but $E^{\circ}_{1/2}$ of **3**, 1.08 V, is about 0.6 V lower than that of durene. This mean that the repulsion integral $4\gamma_1$ in Eq. 18 contributes considerably to the stabilization. If we adopt here $\gamma_1=0.1$ eV, the difference 0.2 eV can be regarded as the contribution from the resonance interaction.

The energy stabilization of **4** and **5** is further enhanced by the eclipsed configuration of the two durene moieties in the center of **4** and orbital mixings of the four durene moieties in **5**, as in the cases of **1** and **2**. $E^{\circ}_{1/2}$ of **4** and **5** clearly show the energy stabilization of the order of 0.9 V.

*Spin Density Distribution.* The transannular interaction in the staggered configuration in **1** does not so much stabilize the system, but induces the mixing between A and S, which results in the spin density redistribution. From the comparison of the observed hfcc with those of the calculated ones, we can estimate $\beta'$ as $0.03\,\beta$. In the previous work,[1m] we also obtained $\beta'=0.03\,\beta$ in the case of coronene trimer cation radical $C_3^{+\cdot}$. It is remarkable that $\beta'$ estimated in the two different systems coincide with each other in spite of the difference of the compounds.

About 0.5 G splittings due to the ring protons in **1** is the same magnitude as that in **2**, but the theoretical calculations (McLachlan and INDO) indicate the opposite sign. This is probably due to the fact that the small transannular interaction between the two moieties induces the spin density redistribution which converts accidentally the sign of usually negative hfcc of −0.5 G.

From the hfcc due to $\mathbf{3}^{+\cdot}$ it was found that the spin density is localized on the central moiety of durene, the ratio of the spin density in the central moiety to that of the side moieties being about 15 : 1. The theoretical treatment of such a mixed layer compound leads to a large apparent $a$, as indicated in Fig. 8. Dessau *et al.* obtained the hfcc of $\mathbf{D}^{+\cdot}$: 10.7 G for the twelve methyl protons and 0.8 G for the two ring protons.[16] The latter is very close to that of the central ring protons in $\mathbf{3}^{+\cdot}$ (0.789 G). Both McLachlan's and INDO calculations support such localization of the spin density, although the hfcc of the side moieties do not agree with the experimental values so well. This probably due to the fact that the hfcc of the side moieties are very sensitive to the distance between the central and side moieties. It is appropriate to conclude that most of the spin density is localized on the central durene moiety in $\mathbf{3}^{+\cdot}$.

The linewidths of $\mathbf{4}^{+\cdot}$ and $\mathbf{5}^{+\cdot}$ show only indirect evidence that the spin density localizes at the central two moieties. The four methyl substitution to **4**, which leads to **5**, produced only a small variation to the linewidth. This suggests small spin distribution on the both side rings and large spin localization on the two central rings of **4**.

The authors wish to express their thanks to Professor Suehiro Iwata of Keio University for his kind suggestions concerning the theoretical treatment of the polymer cation radicals.

## References

1) a) I. C. Lewis and L. C. Singer, *J. Chem. Phys.*, **43**, 2712 (1965); b) O. Howarth and G. K. Fraenkel, *J. Am. Chem. Soc.*, **88**, 4514 (1966); *J. Chem. Phys.*, **52**, 1371 (1970); c) H. van Willigen, E. de Boer, J. T. Cooper, and W. F. Forbes, *ibid.*, **49**, 1190 (1968); d) W. F. Forbes and J. T. Cooper, *Can. J. Chem.*, **46**, 1158 (1968); e) T. C. Chiang and A. H. Reddoch, *J. Chem. Phys.*, **52**, 1371 (1970); f) S. Shih and R. M. Dessau, *ibid.*, **55**, 3757 (1971); g) H. Yoshimi and K. Kuwata, *Mol. Phys.*, **23**, 297 (1972); h) O. Edlund, P. Kinell, A. Lund, and A. Shimizu, *J. Chem. Phys.*, **46**, 3679 (1967); i) P. Kinell and A. Lund, *Acta Chem. Scand*, **26**, 444 (1972); j) T. Ichikawa and P. K. Ludwig, *J. Am. Chem. Soc.*, **91**, 1024 (1969); k) J. Bruhin, F. Gerson, and H. Ohya-Nishiguchi, *Helv. Chim. Acta*, **60**, 2471 (1977); l) F. Gerson, G. Kaupp, and H. Ohya-Nishiguchi, *Angew. Chem., Int. Ed. Engl.*, **16**, 657 (1977); m) H. Ohya-Nishiguchi, H. Ide, and N. Hirota, *Chem. Phys. Lett.*, **66**, 581 (1979).

2) a) B. Badger, B. Brocklehurst, and R. D. Russel, *Chem. Phys. Lett.*, **1**, 122 (1967); b) B. Badger and B. Brocklehurst, *Nature*, **219**, 263 (1968); c) B. Badger and R. D. Russel, *Trans. Faraday Soc.*, **65**, 2159 (1969); d) B. Badger and B. Brocklehurst, *ibid.*, **65**, 2576, 2582, 2588 (1969); **66**, 2939 (1970); e) S. Arai, A. Kira, and M. Imamura, *J. Chem. Phys.*, **56**, 1777 (1972); f) A. Kira, S. Arai, and M. Imamura, *J.*

*Phys. Chem.*, **76**, 1119 (1972); g) M. A. J. Rogers, *Chem. Phys. Lett.*, **9**, 107 (1971); h) M. A. J. Rogers, *J. Chem. Soc., Faraday Trans. 1*, **68**, 1278 (1972).

3) a) M. Meot-Ner(Mautner), P. Hamlet, E. P. Hunter, and F. H. Field, *J. Am. Chem. Soc.*, **100**, 5466 (1978); b) M. Meot-Ner(Mautner), *J. Phys. Chem.*, **84**, 2724 (1980).

4) H. Ohya-Nishiguchi, *Bull. Chem. Soc. Jpn.*, **52**, 2064 (1979).

5) T. Otsubo, S. Mizogami, I. Otsubo, Z. Toyoda, A. Sakagami, Y. Sakata, and S. Misumi, *Bull. Chem. Soc. Jpn.*, **46**, 3519 (1973).

6) T. Otsubo, S. Mizogami, Y. Sakata, and S. Misumi, *Chem. Commun.*, **1971**, 678; *Tetrahedron Lett.*, **1971**, 4803.

7) R. R. Gagne, C. A. Coval, and G. C. Lisensky, *Inorg. Chem.*, **19**, 2854 (1980).

8) B. Kovac, M. Mohraz, E. Heilbronner, V. Boeckelheide, and H. Hopf, *J. Am. Chem. Soc.*, **102**, 4314 (1980), and other references cited therein.

9) F. Gerson, "High Resolution E. S. R. Spectroscopy," John Wiley and Sons Lts. Verlag Chemie (1970), p. 50.

10) N. M. Atherton, "Electron Spin Resonance; Theory and Applications," John Wiley and Sons Inc. New York (1973), p. 105.

11) D. K. Lonsdale, F. R. S., H. J. Milledge, and K. V. K. Rao, *Proc. R. Soc. London, Ser. A*, **255**, 82 (1960).

12) Y. Koizumi, T. Toyoda, H. Horita, and S. Misumi, presented at the 22nd National Meeting of the Chemical Society of Japan, Tokyo, April 1975, Summary I, p. 184.

13) For example, J. A. Pople and D. L. Beveridge, "Approximate Molecular Orbital Theory," McGraw-Hill Inc. (1970).

14) S. Iwata, private communication.

15) E. Hückel, *Z. Phys.*, **76**, 628 (1932).

16) R. M. Dessau, S. Shih, and E. I. Heiba, *J. Am. Chem. Soc.*, **92**, 412 (1970).